Three-dimensional electromagnetic model of the pulsed-power *Z*-pinch accelerator

D. V. Rose,* D. R. Welch, E. A. Madrid, C. L. Miller, and R. E. Clark

Voss Scientific, LLC, Albuquerque, New Mexico 87108, USA

W. A. Stygar, M. E. Savage, G. A. Rochau, J. E. Bailey, T. J. Nash, M. E. Sceiford, and K. W. Struve

Sandia National Laboratories, Albuquerque, New Mexico 87185, USA

P. A. Corcoran and B. A. Whitney

L-3 Communications, San Leandro, California 94577, USA

A three-dimensional, fully electromagnetic model of the principal pulsed-power components of the 26-MA ZR accelerator [D. H. McDaniel *et al.*, in *Proceedings of the 5th International Conference on Dense Z-Pinches* (AIP, New York, 2002), p. 23] has been developed. This large-scale simulation model tracks the evolution of electromagnetic waves through the accelerator's intermediate-storage capacitors, laser-triggered gas switches, pulse-forming lines, water switches, triplate transmission lines, and water convolute to the vacuum insulator stack. The insulator-stack electrodes are coupled to a transmission-line circuit model of the four-level magnetically insulated vacuum-transmission-line section and double-post-hole convolute. The vacuum-section circuit model is terminated by a one-dimensional self-consistent dynamic model of an imploding *z*-pinch load. The simulation results are compared with electrical measurements made throughout the ZR accelerator, and are in good agreement with the data, especially for times until peak load power. This modeling effort demonstrates that 3D electromagnetic models of large-scale, multiple-module, pulsed-power accelerators are now computationally tractable. This, in turn, presents new opportunities for simulating the operation of existing pulsed-power systems used in a variety of high-energy-density-physics and radiographic applications, as well as even higher-power next-generation accelerators *before* they are constructed.

PACS numbers: 52.58.Lq, 84.70.+p, 52.65.Rr

I. INTRODUCTION

Electrostatic (ES) and electromagnetic (EM) models of pulsed-power-accelerator components have been important tools in the design and analysis of pulsed-power systems for a number of years (see, for example, Refs. [1–5]). Used in concert with other computational modeling tools such as transmission-line and circuit codes, ES and EM codes have been successfully used in the design and optimization of a number of large-scale pulsed-power facilities, notably the ZR *z*-pinch accelerator at Sandia National Laboratories [6–16].

The ZR accelerator, which is a significant refurbishment of the highly successful *Z* machine [17–22], drives a variety of loads, including *z* pinches [23–25], isentropic compression [26,27], and flyer plates [28,29]. These experimental capabilities support ongoing research in inertial-confinement-fusion [30–37], magnetohydrodynamics [38], radiation-effects [39], radiation-physics [40,41], astrophysics [42], equation-of-state [43–46], pulsed-power-physics [47], and other high-energy-density-physics experiments [24,48].

The ZR accelerator is located in a tank that is 6 m tall and has an outer diameter of 33 m. The accelerator in-

cludes 36 pulsed-power modules which are electrically in parallel. Two of the modules are illustrated by Fig. 1. The modules are arranged in two levels, with 18 modules in each level. The modules are arranged symmetrically
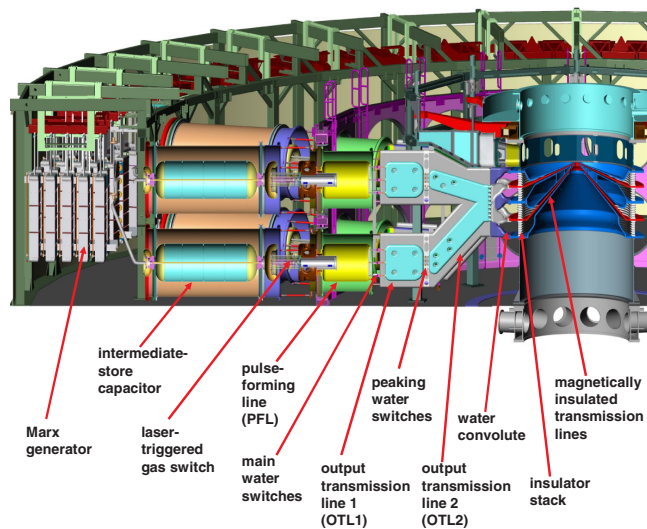
FIG. 1. (Color) Cutaway view of the ZR accelerator at Sandia National Laboratories. Principal components of the accelerator are labeled.

*David.Rose@vosssci.com

around the centrally located vacuum section, which consists of the insulator stack and a system of four parallel magnetically insulated transmission lines (MITLs). The electrical power pulses generated by the 36 modules are delivered to the four MITLs. The currents in the MITLs are added via a double-post-hole vacuum convolute; the combined current is delivered to a single radial vacuum transmission line that, in turn, delivers the current to the centrally located load.

The electrical energy that is ultimately delivered to the load is initially stored in the capacitors of ZR's 36 Marx generators, which are electrically in parallel. The Marx generators include a total of 2160 capacitors rated at 2.6-μF. ZR has as many Marx capacitors as Z did, but each ZR capacitor has twice the capacitance. Hence, at a given Marx-charge voltage, the ZR Marxes store twice the energy. The Marx generators are simultaneously DC charged in ~100 s, and are discharged in ~1 μs into 36 water-insulated intermediate-energy-storage capacitors.

When the voltage on each intermediate-storage (IS) capacitor is near its peak value, the IS is discharged through a laser-triggered gas switch into a water-insulated pulse-forming line (PFL). Individual laser triggering of the switches (i.e., one laser per switch) allows for programmable pulse shaping on each shot. The energy in each PFL is subsequently discharged, through three self-break water switches, into a water-insulated vertical triplate transmission line. We refer to this as the first output transmission line, or OTL1 (Fig. 1). The OTL1 in turn discharges through four self-break water-insulated pulse-sharpening gaps into the second output transmission line (OTL2).

As suggested by Fig. 1, the OTL2 from an upper module merges with the OTL2 from the module below to form a single triplate transmission line that delivers the power pulses from the two paired modules to the water convolute (18 such transmission lines deliver the 36 power pulses to the convolute). The convolute connects to the insulator stack, which in turn connects to the MITL system. The MITLs (which are located inside the stack) converge upward to elevate the load above the pulsed-power components of the accelerator, enabling improved diagnostic access.

Here we describe a new EM computational modeling capability that is being used to analyze the propagation of EM waves through the principal pulsed-power components of the ZR accelerator. The 3D EM particle-in-cell (PIC) code LSP [49] is used to model EM wave propagation in the oil and water sections of ZR. Although inherently a PIC code designed for solving plasma physics problems [50,51], LSP has a number of features that make it a suitable choice for this particular application, including internal implementation of the BERTHA transmission-line code [52], complex geometric constructs, time-dependent material properties, a variety of ES and EM field solvers, and a flexible two-level domain decomposition scheme for par-

allel execution. With the addition of several new features including a scheme for handling spatial conversion of the mesh from cylindrical to Cartesian coordinates, this new simulation capability compliments existing numerical tools, such as finite element and transmission-line codes. Together these tools will assist in the design and deployment of next-generation, large-scale, pulsed-power facilities for *z*-pinch research such as the proposed 1000-TW ZX facility [4,53,54].

This paper is organized as follows. Section II presents an overview of the numerical model and describes several novel numerical techniques implemented in the EM simulations. In Sec. III, direct comparisons between the measured electrical signals from ZR-shot 1896 and numerical-model results are given. A summary and discussion of several possible refinements to the modeling are given in Sec. IV.

II. MODEL

The model presented here is composed of two parts: a 3D EM simulation region modeling the oil and water sections and a transmission-line region that models the vacuum sections. As described below, these two parts are dynamically coupled within the LSP model. The simulations are carried out in 3D cylindrical coordinates (r, θ, z) to model the ZR accelerator (the coordinate system changes to Cartesian at large radius, as described below). We note that LSP has been used to model a number of pulsed-power accelerators including the Sandia LTDR [55], a 1-MV linear-transformer driver, and the Sandia RITS-6 accelerator [56–58], a 12-MV inductive voltage adder. In these examples, LSP PIC simulations were used to model the evolution of electron power flow along MITLs, with EM power driven into the system through transmission-line-circuit representations of the pulsed-power sections. In addition, LSP has been utilized in a number of studies of high-power MITLs [59–64] to motivate and validate theoretical models of electron power flow.

The EM portion of the 3D LSP model of ZR represents a single sector of ZR, which includes two of ZR's 36 pulsed-power modules, as illustrated in Fig. 2. The LSP simulations[1] are conducted on a 3D finite grid that extends radially from $r = 1.45$ m to 16.5 m. The grid is composed of approximately 21.7×10^6 cells, with an average spatial resolution of ~2 cm. The upper and lower boundaries are modeled as conductors, although in ZR the upper boundary includes complex oil/air and water/air interfaces that can

---

[1]Each simulation used 144 processors on the Sandia National Laboratories (SNL) Thunderbird computer system and required approximately 24 hours of total run time. This computer system was designed and built by SNL and Dell [65] and contains 8960 Intel [66] Xeon processors operating at 3.6 GHz and uses the Infiniband interconnect architecture [67].
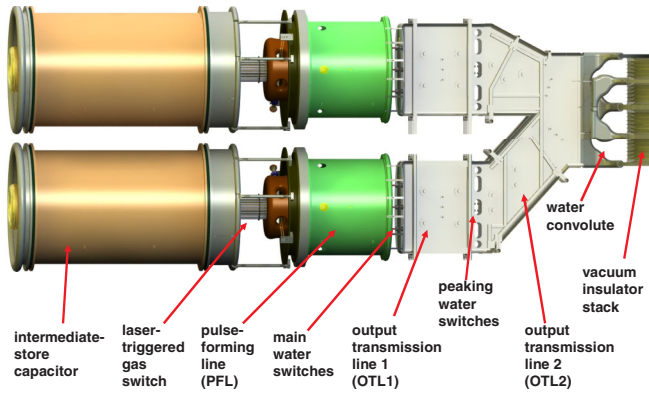
FIG. 2. (Color) Schematic of two pulse-forming sections of ZR with principal components labeled (dimensions in centimeters). Not shown here are the vacuum MITLs and load region.

electrically flash during a shot. The azimuthal extent of the simulation model is 20 degrees, or 1/18th of the entire machine. The ZR insulator stack and MITLs are cylindrically symmetric from the vacuum post-hole convolute to the water convolute; i.e., for radii between 0.1 and 2 m. Cylindrical symmetry is broken for radii beyond the water-convolute region ($r \sim 2$ m), outside of the insulator stack, where the parallel-plate output transmission lines of the individual modules combine in the water convolute. At $r_t = 5.8$ m, at the set of water switches (WS) located between the PFL and OTL1 components, the computational grid metric changes from cylindrical to Cartesian. This fixes the θ-direction cell dimension at radii larger than r_t at ~ 1.8 cm, and enables the coaxial anode-cathode gaps in the IS and PFL components (which are essentially coaxial capacitors) to be modeled in Cartesian coordinates with finite grid-cell dimensions in all three directions of ~ 2 cm. Thus no abrupt numerical transitions in the power flow direction are introduced that could cause spurious reflections. This transition region in the computational grid was extensively analyzed and no evidence of wave reflections was found. This is likely due to the fact that the change in the coordinate system metric at this large radius is relatively small, although accurate to only first order.

The upper and lower IS capacitors [68] are treated as precharged water-dielectric components in the model. A relative dielectric constant of 80 and a measured electrical conductivity of 2.7×10^5 s^{-1} are assumed for the water in the IS capacitors. Energy is released from the IS capacitors once the laser-triggered gas switches (LTGS) [9,12,16,69,70] are fired (at $t = 2$ ns in the model). Energy is transferred from the IS to water-insulated PFL, which then discharges through a set of self-break water switches [71,72] into OTL1. In the ZR design, the transition from the coaxial PFL to the triplate OTL1 is done abruptly at the first set of water switches to minimize reflections and to conserve radial length [73,74]. The OTL1 discharges through a set of self-break pulse-

sharpening water switches into OTL2, which in turn delivers power to the water convolute. The water insulator of the PFLs, OTL1s, OTL2s, and water convolute has a relative dielectric constant of 80, and a measured electrical conductivity of approximately 1.8×10^6 s^{-1}. The reduced water resistivity in this section is used to help dissipate energy that is reflected from the stack-MITL system. Each of the two ZR modules in the simulation model includes a single LTGS, three WSs, and four pulse-sharpening water switches (PSWS).

The electrical power generated by the upper and lower modules is transferred from the machine's water section to the vacuum section through the vacuum insulator stack. Four electrically parallel conical MITLs deliver electrical power from the stack to the central region of the machine [18–20]. Post-hole convolutes combine the currents from these transmission lines to a single 6-cm-long radial-disk feed that drives the z-pinch load. The computational model uses an integrated transmission-line network, based on the BERTHA code [52], to model most of the vacuum section of the machine, from the vacuum side of the insulator stack (beginning at $r = 145$ cm) to the load ($r = 0$). This transmission-line circuit [10,75] is illustrated in Fig. 3. Table I gives the values for the transmission-line elements shown in the figure. Electromagnetic waves are coupled to the circuit at the downstream side of the insulator stack (left-hand side of the figure), and drive four independent radial transmission lines (labeled in the figure as the vacuum-flare and MITL sections). The four MITLs are combined through the post-hole convolutes; the output power drives a load. A 1D self-consistent dynamic load model (see, for example, Appendix A of Ref. [5]) incorporating multiple, nested wire arrays imploding on a foam core [76–79] is used for the analysis of ZR-shot 1896. The load is 1.2 cm long and comprised of two nested wire arrays at radii of 2.0 cm and 1.0 cm with masses 4.46 mg
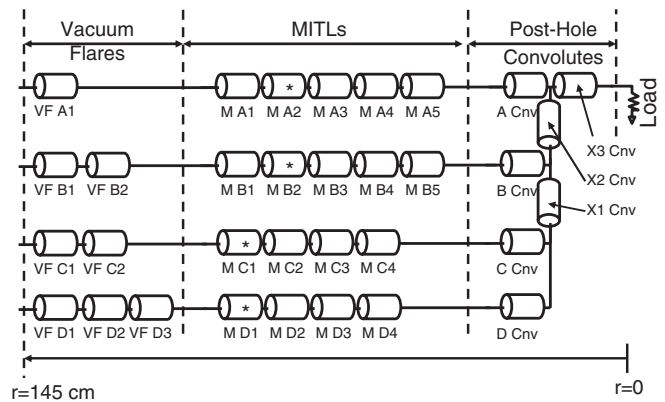
FIG. 3. Schematic of the transmission-line equivalent circuit model used in the LSP simulation to model the ZR accelerator's vacuum section and load. The starred elements indicate the measurement position for the MITL currents. Values for the various elements are given in Table I.

TABLE I. Circuit element parameters used in the vacuum section of the model. The MITL currents shown in Fig. 3 are measured across elements M A2, M B2, M C1, and M D1. The effective outer radius for each of the vacuum flare and MITL elements is also given.

Element	Impedance (Ohms)	Length (ns)	Outer radius (cm)
VF A1	5.28	0.457	145.1
VF B1	8.58	0.208	145.1
VF B2	4.86	0.834	140.4
VF C1	10.97	0.352	145.1
VF C2	4.90	0.471	134.1
VF D1	9.87	0.621	145.1
VF D2	8.92	0.463	134.6
VF D3	6.93	0.345	127.4
M A1	2.33	1.38	131.4
M A2	2.46	0.998	93.4
M A3	2.70	1.01	66.3
M A4	3.08	0.498	38.5
M A5	3.97	0.504	24.8
M B1	2.41	1.11	121.0
M B2	2.55	1.00	91.4
M B3	2.80	1.00	64.6
M B4	3.19	0.502	38.0
M B5	4.05	0.506	24.5
M C1	3.28	3.56	123.2
M C2	3.89	1.00	51.4
M C3	2.63	0.508	31.2
M C4	4.26	0.504	21.1
M D1	3.30	3.81	121.5
M D2	3.45	1.00	49.4
M D3	3.73	0.508	30.3
M D4	4.37	0.50	20.6
A Conv	2.66	1.00	
B Conv	0.573	1.00	
C Conv	3.84	1.00	
D Conv	2.35	1.00	
X1 Conv	1.09	1.00	
X2 Conv	1.11	1.00	
X3 Conv	3.21	1.00	

and 2.23 mg, respectively. A low-density foam core of radius 0.3 cm is placed on axis and is treated in the model simply as five equal mass concentric shells. The load is a dynamic hohlraum, designed to include a fusion fuel capsule in the center of the foam core.

The connection between the EM simulation grid through a first-order wave-transmitting boundary into the transmission-line model requires essentially transverse-electromagnetic (TEM)-only modes. To accomplish this, we artificially extend the radial transmission lines that pass through the vacuum insulator stack. The lines extend from $r = 170.3$ cm to $r = 156.6$ cm, and include a Rexolite insulator with a relative dielectric constant of 2.55. We artificially extend the lines inward to $r = 145$ cm. This

extension provides additional propagation distance to symmetrize the EM waves emerging through the insulator stack. In addition, we impose a nonzero longitudinal conductivity on the dielectrics of the insulator stack and the vacuum region leading to the grid-to-transmission-line junction at $r = 145$ cm. We assume for this region that the dielectric has a constant conductivity of 10^{11} s^{-1}, in the radial direction only, to remove additional non-TEM components from all EM waves incident on the junction. Without these constructs, EM wave coupling at the junction results in unphysically large voltage oscillations along the vacuum transmission line and load. The conductivity value used here was determined empirically and found to be (approximately) the minimum requisite value.

The switch models used in the simulation assume fixed-volume regions with temporal resistivity functions to emulate the closing of the LTGS, WS, and PSWS. These simple functions are empirically determined and tested using transmission-line models of ZR [10]. These switch resistance functions result in the correct timing and dynamic response of the major pulsed-power components. (See Fig. 5 for a plot of the switch resistances used in the simulations.) The LSP model does not account for the inductance evolution of these switches (which would require much finer spatial resolution due to the complex electrical breakdown of the gas or water channels in these devices), but this appears to be a relatively small effect on the overall EM power flow dynamics in the model.

As part of the development of the simulation model, we utilized calculation results from the TLCODE [80], a transmission-line-circuit code that has been used to model both the Z [18,20] and ZR accelerators [10]. The TLCODE model results can either use precharged IS capacitors or include a model of the Marx banks used to charge these capacitors.

III. SIMULATION RESULTS

We used the LSP model of ZR to simulate ZR-shot 1896, a dynamic nested-wire-array z-pinch shot with an 82-kV Marx charge. Unless otherwise noted, the measured electrical signals in the oil and water sections shown below are taken from ZR module 17 (of 36). In the LSP simulations discussed here, the upper and lower IS capacitors are precharged to 6.2 MV, which is higher than the average peak value of about 5.6 MV measured on the 36 IS capacitors for shot 1896. Since we do not include the time-dependent Marx charging of the IS capacitors in the LSP model at this time, we increase the IS voltage by 11% to account for the additional charge that is driven into the IS capacitors from the discharging Marx banks *after* the LTGSs fire. The precharge voltage value of 6.2 MV was determined from the TLCODE simulations discussed in Sec. II.

In Fig. 4, the measured voltages from the upper module (a) IS, (b) PFL, (c) OTL1, and (d) OTL2 are shown along with the LSP simulation results. In Fig. 4(a), the falling IS
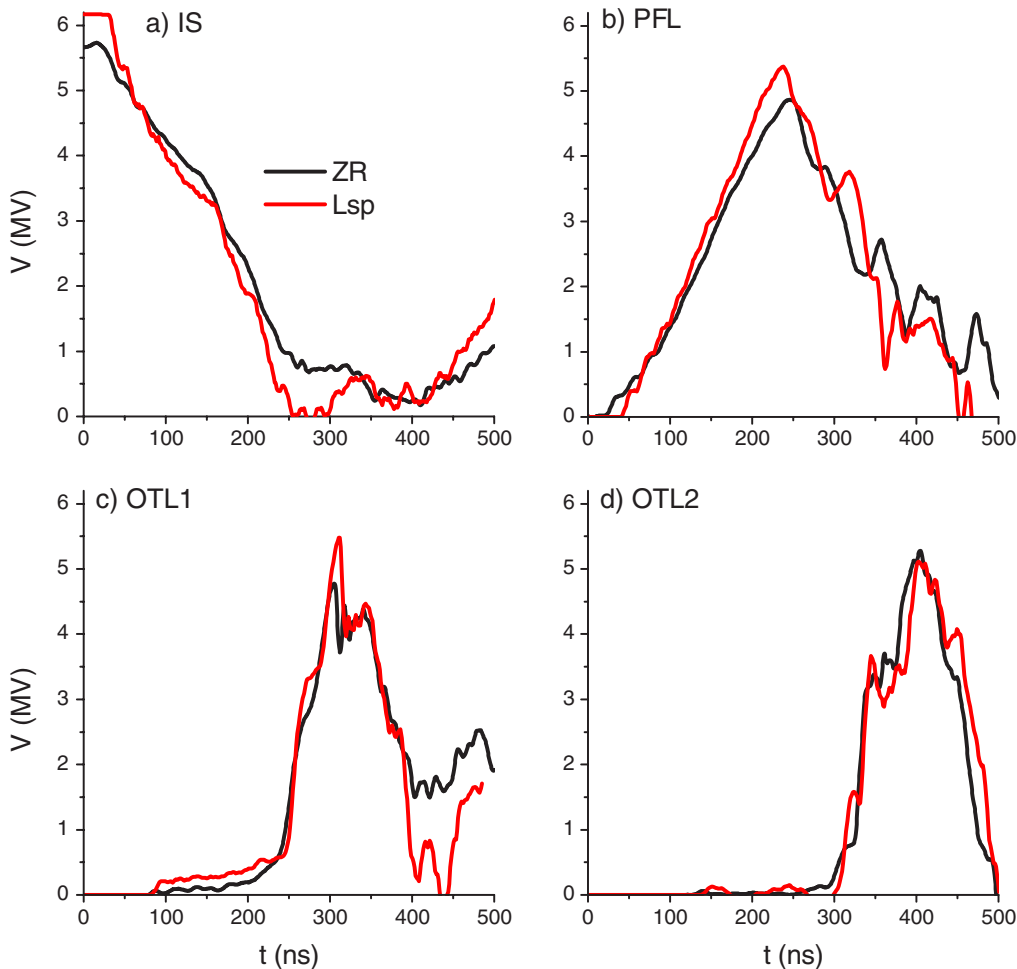
FIG. 4. (Color) Comparison of voltages between ZR-shot 1896 data, module 17 (black curves), and LSP simulation (red curves) for the upper (a) IS, (b) PFL (c) OTL1, and (d) OTL2.

voltage indicates the firing of the LTGS, which transfers stored energy forward through the LTGS into the PFL. The measured falling voltage in the IS capacitor is in reasonable agreement with the simulated value until ~240 ns, when the WSs close. Energy stored in the PFL begins to discharge once the first set of WSs closes [Fig. 4(b)] and charge the OTL1 section. Here the simulated peak voltage on the PFL is higher than the measured value, consistent with the initial overcharging of the IS capacitor in the simulation. The measured and simulated discharge times of the PFL between 250 and 400 ns are similar, although the individual fluctuations seem to be somewhat out of phase. At $t \sim 290$ ns, the PSWSs close and energy flows out of OTL1 [Fig. 4(c)] and into OTL2 [Fig. 4(d)]. Here the measured and simulated voltages are in good agreement, with similar average peak values and pulse widths. This agreement demonstrates that the initial overcharging of the IS capacitors gives results (further downstream) that are consistent with the model of continued Marx discharge after LTGS triggering.

Figure 5 plots the individual switch resistances in the simulations. These values are computed by directly mea-

suring the voltage $V(t)$ across the switch gap and measuring the current $I(t)$ flowing through the electrode immediately upstream of the gap. The resistance is obtained from

$$R(t) = \frac{V(t)}{I(t)} - \frac{L_s}{I(t)} \frac{dI(t)}{dt},$$

where L_s is a constant inductance, empirically determined to give a nearly flat value of $R(t)$ around the time of peak power in switch. Values for L_s obtained by this analysis are 3.0 nH for LTGS, 1.5 nH for the WS, and 0.4 nH for the PSWS. These values are consistent with simple analytic estimates of the conductivity channel dimensions used in the simulation switch models. The switch resistances plotted by Fig. 5 illustrate both the effective closure time of the switch as well as the time during which significant current is actually flowing through each switch. During the times of peak power passage through each of the switch stages, a relatively low variation in the measured switch-to-switch resistance is obtained.

Voltage and current measurements at the insulator stack are shown in Figs. 6(a) and 6(b). The simulated stack
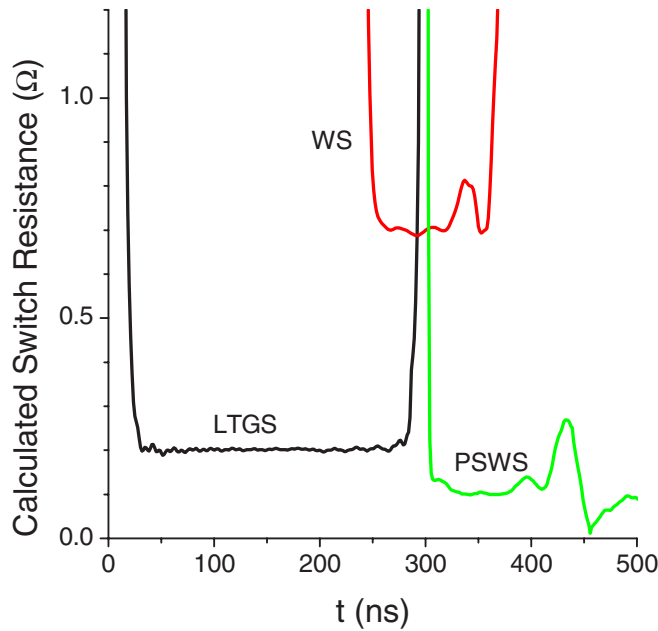
FIG. 5. (Color) Individual switch-resistance time histories inferred from the simulation.

voltage shown here has been smoothed to facilitate comparison to the average of the 18 level-A *V*-dot monitors [81], which are arranged at different azimuthal positions around the machine. High-frequency electric-field oscillations can occur in the simulation in part as a result of the somewhat limited spatial resolution that is used in the model. We note that several of the individual measured signals (not shown here) exhibit oscillations that are consistent with the simulated voltages, while other signals give a smoother response, consistent with the average shown in Fig. 6. The reason for these variations in the measured stack voltages is not known. A possible future application of this model would be adding several modules in azimuth to study module-to-module coupling at the water convolute and insulator stack including any effects due to jitter. Interestingly, the measured stack current rise times, shown in Fig. 6(b), are consistent with the simulated currents at the stack for all four levels (the sum of the currents at all four levels is shown here). However, the peak simulated value exceeds the measured value somewhat. This is also true in the comparison of the MITL and load currents, shown in Figs. 6(c) and 6(d), respectively. The relatively
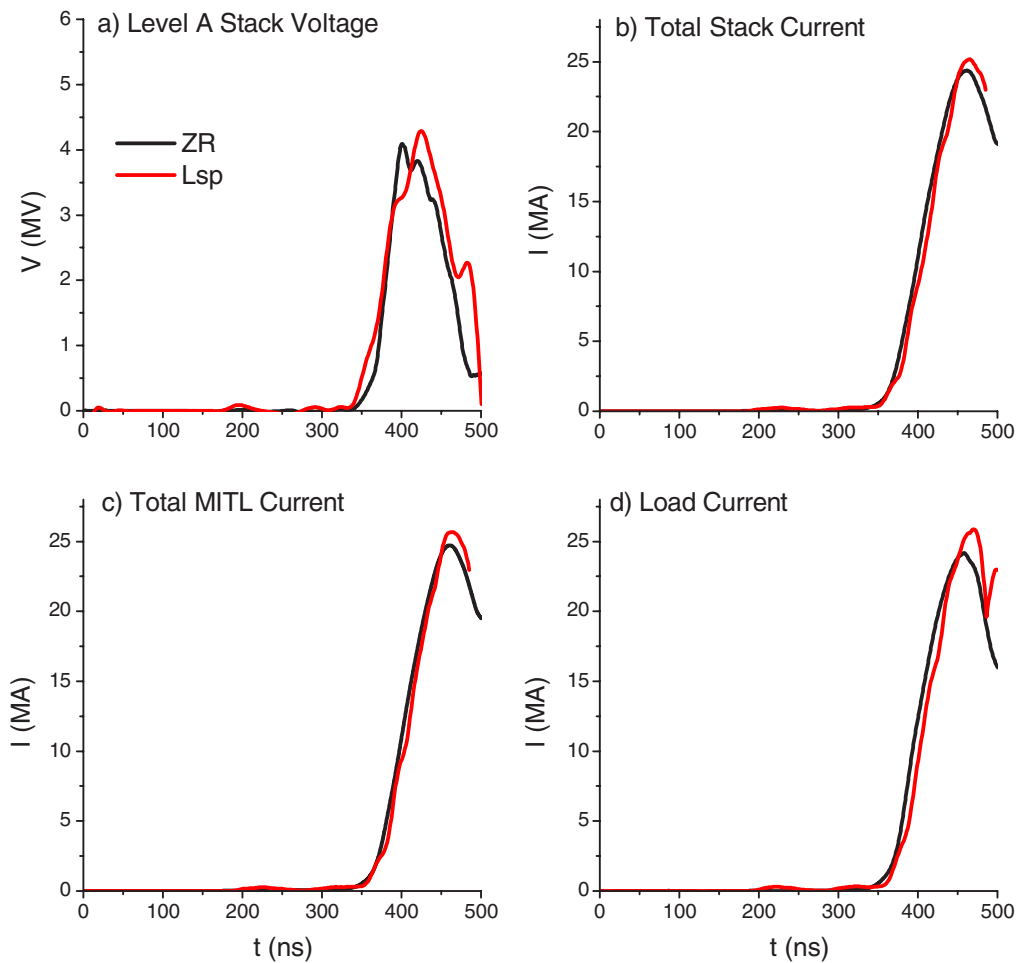
FIG. 6. (Color) Comparison of measured and simulated electrical signals at (a), (b) the insulator stack, level A, (c) the current in the level A MITL, and (d) the load current.

simple transmission-line model of the vacuum section of ZR, shown in Fig. 3, does not account for the current losses that occur in the vicinity of the post-hole convolute. These losses are likely to be the result of complex plasma formation and dynamics, which is sensitive to the load impedance [5,14]. Additional current losses in the MITLs due to Ohmic heating, magnetic diffusion, and $\mathbf{j} \times \mathbf{B}$ work are not included here [47,82] and may contribute to the differences between the simulated and measured currents. In addition, the load model used here is a simple multiple-shell snow-plow model that does not correctly treat all of the dynamics of the actual wire-array pinch evolution.

The 3D LSP simulation model also provides a visual aid to EM energy flow, dissipation, and reflections in the system. Figure 7 is a sequence of four frames from a movie of electric-field magnitudes in the system. Note that we have truncated the radial view in these frames at 14 m to improve visualization of the main accelerator components. At $t = 1$ ns, the precharged IS capacitors clearly show the stored energy, which is about to be released through the closing of the LTGS. After 220 ns, the PFLs are almost completely charged and the WSs between the PFLs and the OTL1 triplates are closing. Residual energy remaining in the IS capacitors is visible at this time. At 300 ns, the
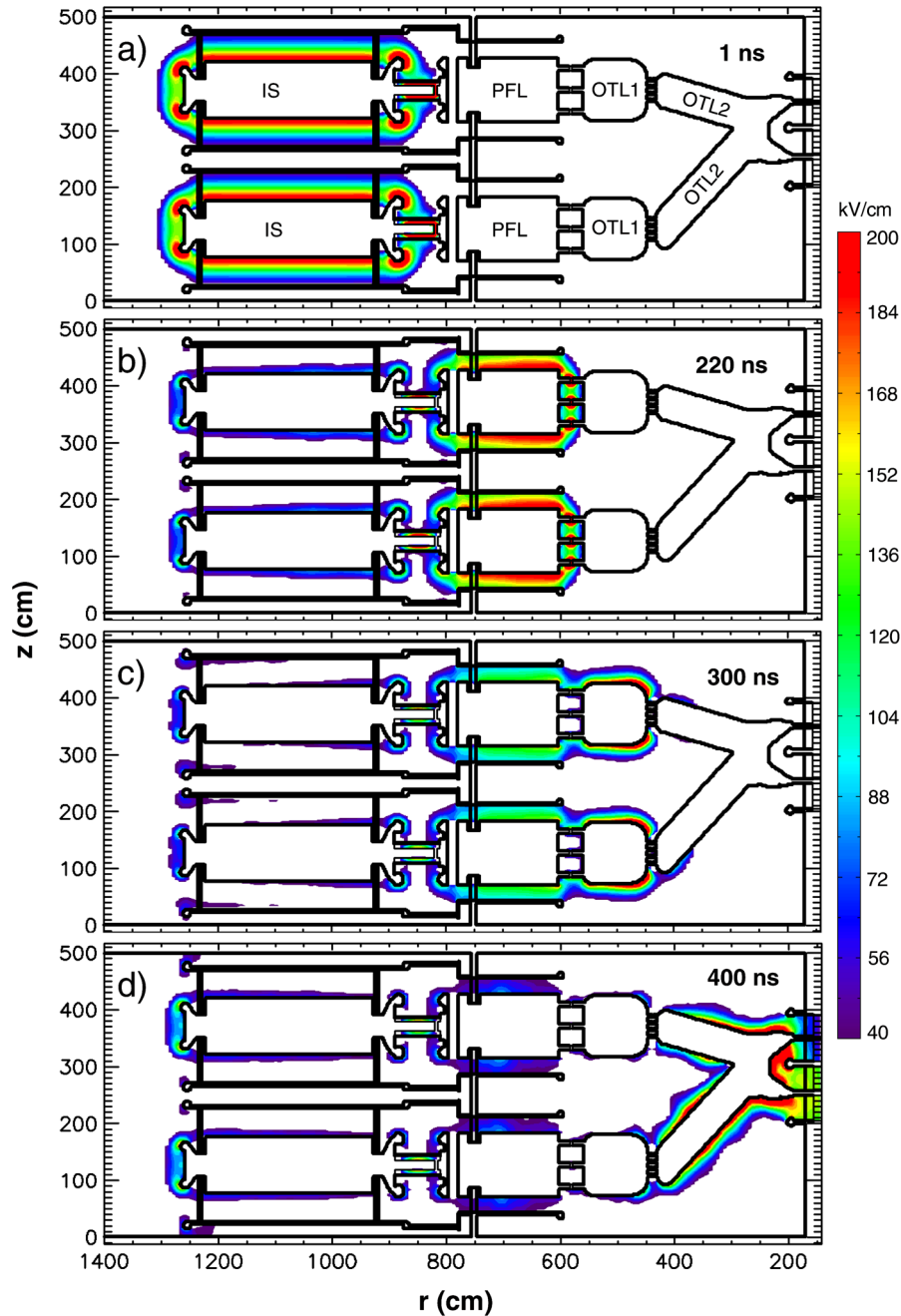
FIG. 7. (Color) Electric-field magnitude in the LSP ZR simulation at times 1, 220, 300, and 400 ns in the $\theta = 0$ plane.
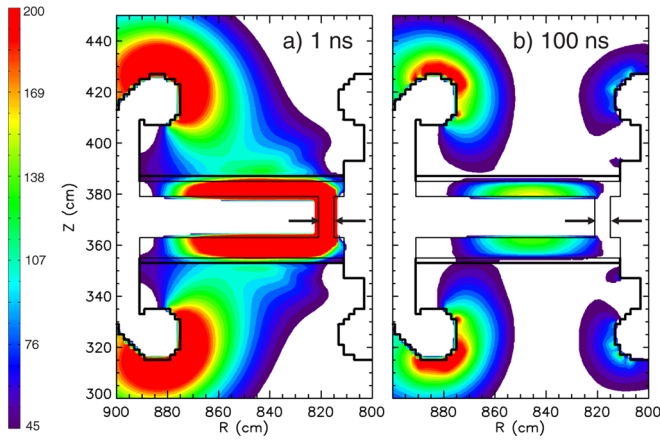
FIG. 8. (Color) Electric-field magnitude in the upper module laser-triggered gas switch in the $\theta = 0$ plane at 1 and 100 ns. The arrows indicate the location of the conductivity channel in the switch.

FIG. 9. (Color) Electric-field magnitude in the upper module water switches in the $\theta = 0$ plane at 200 and 300 ns. The arrows indicate the location of the conductivity channel in the switch.

PSWSs between the OTL1 and OTL2 sections are beginning to close, and energy stored in OTL1 is just beginning to flow into OTL2. Finally after 400 ns, the power pulse is passing through the water convolute and insulator stack. This last frame also illustrates residual and reflected EM power remaining in the system.

Detailed views of the switches in the upper module are given in Figs. 8–10. These views illustrate the relatively simple geometric switch representations used in the simulation model. In each figure, a set of arrows indicates approximate location of the conductivity channel used to close the switch at the times indicated in Fig. 5. The LTGS section which connects the IS to the PFL is shown in Fig. 8. This section includes approximate representations of the electric-field shapers outside the switch, but simplifies the overall complex two-stage breakdown sections in the LTGS as a single gap. The rise time of the electrical conductivity in the single gap approximates the total breakdown time of the LTGS. The WS section which connects the PFL and OTL1 sections is shown in Fig. 9. This section is comprised of three individual switches, which all close simultaneously in the model. On ZR, these self-breakdown switches are comprised of spherical electrodes mounted on cylindrical stalks. Here the finite grid size is too coarse to accurately model these shapes, but the interelectrode gaps are approximately those used on ZR. Finally, the PSWS section connecting the OTL1 and OTL2 components is shown in Fig. 10. This section includes four individual water switches, and once again the finite grid size is too coarse to model these shaped conductors.

Overall, the LSP results are in good agreement with the ZR voltage and current measurements; the waveforms have similar temporal profiles and amplitudes throughout the accelerator stages. A separate simulation of ZR shot 1780, which used a short-circuit load, gives a peak load current of 26.2 MA and a load-current rise time (10%–90%) of
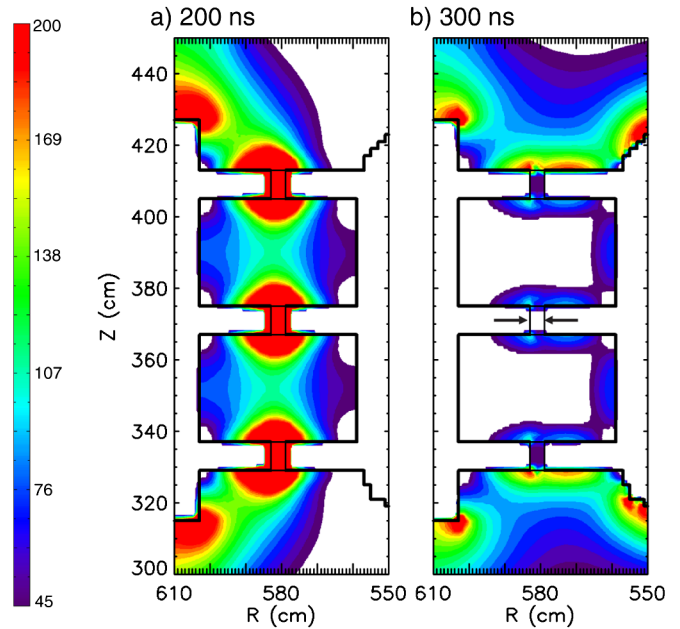
$\sim$76 ns. These results are in good agreement with the measured ZR load current with a peak value of 26.4 MA and $\sim$81 ns rise time. This supports the supposition mentioned above that measured current losses in the post-hole
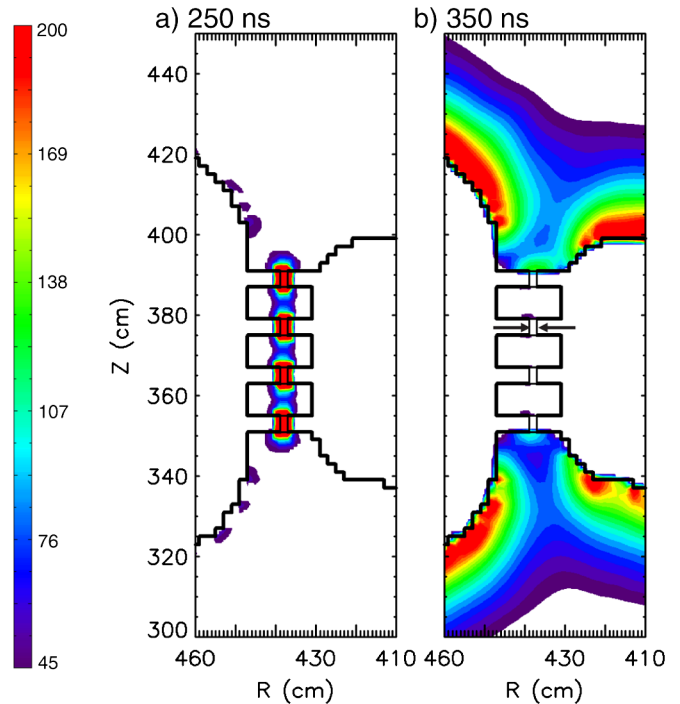
FIG. 10. (Color) Electric-field magnitude in the upper model pulse-sharpening water switches in the $\theta = 0$ plane at 250 and 350 ns. The arrows indicate the location of the conductivity channel in the switch.

convolute due in part to the dynamic impedance of wire-array load could lead to EM wave reflections in the MITL section that are not included in the vacuum-transmission-line section of the model. Further analysis is required to understand the differences between the measured and simulated waveforms in the vacuum sections of ZR.

IV. SUMMARY

A new 3D model of EM wave propagation in the ZR accelerator has been developed using the LSP code. The model has been used to simulate the electrical performance of a ZR shot taken with a dynamic wire-array *z*-pinch load. Detailed comparisons with measured electrical signals throughout the accelerator have been carried out and show overall agreement. Several computational techniques have been developed, implemented, and tested within the model to complete these large-scale simulations. These include the development of a technique to change the coordinate system of the underlying mesh from cylindrical to Cartesian at a predetermined radius, and a model for reducing non-TEM modes at the junction between the 3D PIC grid and the 1D transmission-line model.

A significant result of this work is the demonstration that 3D models of large-scale, multiple-module pulsed-power accelerators are now computationally tractable. Such models will be important design tools for future large-scale systems, enabling the construction of *virtual* accelerators, which would complement existing modeling tools such as lumped-circuit and transmission-line models. The 3D models would be used to perform fully electromagnetic simulations of the performance of complete, entire super-power accelerators, before they are constructed.

This paper reports on the application of such a model to the ZR accelerator, demonstrating good agreement with measured waveforms for times up to peak load power. Future work will focus on refinements to the switch models used in these calculations. In particular, the time-dependent physics of the evolving arcs and gas dynamics in these switches is complex [9,69–72] and is not treated here. More detailed models of these components will likely improve the overall utility of the model. In addition, future work will include improved circuit representations of the inner portions of the machine, including the vacuum transmission lines, post-hole-convolute, and dynamic loads. In addition, a transmission-line representation of the Marx charging circuit will be added to include effects due to the dynamic charging of the intermediate storage.

[1] R. W. Shoup, F. Long, T. H. Martin, R. B. Spielman, W. A. Stygar, M. A. Mostrom, K. W. Struve, H. Ives, P. Corcoran, and I. Smith, in *Proceedings of the 11th IEEE International Pulsed Power Conference, Baltimore, MD, 1997*, edited by G. Cooperstein and I. Vitkovitsky (IEEE, Piscataway, NJ, 1997), p. 1608.

[2] T. D. Pointon, W. A. Stygar, R. B. Spielman, H. C. Ives, and K. W. Struve, Phys. Plasmas **8**, 4534 (2001).

[3] R. B. Spielman, in *Proceedings of the 27th Power Modulator Symposium, Arlington, VA, 2006*, edited by R. J. Umstattd (IEEE, Piscataway, NJ, 2006), p. 43.

[4] D. R. Welch, T. C. Genoni, D. V. Rose, N. Bruner, and W. A. Stygar, Phys. Rev. ST Accel. Beams **11**, 030401 (2008).

[5] D. V. Rose, D. R. Welch, T. P. Hughes, R. E. Clark, and W. A. Stygar, Phys. Rev. ST Accel. Beams **11**, 060401 (2008).

[6] D. H. McDaniel, M. G. Mazarakis, D. E. Bliss, J. M. Elizondo, H. C. Harjes, H. C. Ives, D. L. Kitterman, J. E. Maenchen, T. D. Pointon, S. E. Rosenthal, D. L. Smith, K. W. Struve, W. A. Stygar, E. A. Weinbrecht, D. L. Johnson, and J. P. Corely, in *Proceedings of the 5th International Conference on Dense Z-Pinches*, edited by J. Davis (AIP, New York, 2002), p. 23.

[7] E. A. Weinbrecht, D. D. Bloomquist, D. H. McDaniel, G. R. McKee, G. L. Donovan, J. W. Weed, T. V. Faturos, D. A. Tabor, and C. Moncayo, in *Proceedings of the 16th IEEE Pulsed Power and Plasma Science Conference, Albuquerque, NM, 2007*, edited by E. Schamiloglu and F. Peterkin (IEEE, Albuquerque, New Mexico, 2007), p. 975.

[8] M. E. Savage, L. F. Bennett, D. E. Bliss, W. T. Clark, R. S. Coats, J. M. Elizondo, K. R. LeChien, H. C. Harjes, J. M. Lehr, J. E. Maenchen, D. H. McDaniel, M. F. Pasik, T. D. Pointon, A. C. Owen, D. B. Seidel, D. L. Smith, B. S. Stoltzfus, K. W. Struve, W. A. Stygar, L. K. Warne, J. R. Woodworth, C. W. Mendel, K. R. Prestwich, R. W. Shoup, D. L. Johnson, J. P. Corley, K. C. Hodge, T. C. Wagoner, and P. E. Wakeland, in Proceedings of the 16th IEEE Pulsed Power and Plasma Science Conference, Albuquerque, NM, 2007 (Ref. [7]), p. 979.

[9] K. R. LeChien, M. E. Savage, V. Anaya, D. E. Bliss, W. T. Clark, J. P. Corley, G. Feltz, J. E. Garrity, D. W. Guthrie, K. C. Hodge, J. E. Maenchen, R. Maier, K. R. Prestwich, K. W. Struve, W. A. Stygar, T. Thompson, J. Van Den Avyle, P. E. Wakeland, Z. R. Wallace, and J. R.

Woodworth, Phys. Rev. ST Accel. Beams **11**, 060402 (2008).

[10] P. A. Corcoran, B. A. Whitney, V. L. Bailey, L. G. Schlitt, M. E. Seiford, J. W. Douglas, M. E. Savage, W. A. Stygar, and I. D. Smith, in *Proceedings of the 17th IEEE International Pulsed Power Conference, Washington, DC, 2009* (IEEE, Piscataway, NJ, 2009), p. 150.

[11] M. E. Savage and B. S. Stoltzfus, Phys. Rev. ST Accel. Beams **12**, 080401 (2009).

[12] K. LeChien, W. Stygar, M. Savage, R. McKee, D. Bliss, P. Wakeland, D. Artery, M. Baremore, P. Jones, S. Roznowski, and S. White, in Proceedings of the 17th IEEE International Pulsed Power Conference, Washington, DC, 2009 (Ref. [10]), p. 604.

[13] J. Lips, J. Garde, A. Owen, R. McKee, and W. Stygar, in Proceedings of the 17th IEEE International Pulsed Power Conference, Washington, DC, 2009 (Ref. [10]), p. 1266.

[14] D. V. Rose, D. R. Welch, R. E. Clark, E. A. Madrid, C. L. Miller, C. Mostrom, W. A. Stygar, M. E. Cuneo, C. A. Jennings, B. Jones, D. J. Ampleford, and K. W. Struve, in Proceedings of the 17th IEEE International Pulsed Power Conference, Washington, DC, 2009 (Ref. [10]), p. 1153.

[15] B. Stoltzfus, K. LeChien, M. Savage, and W. Stygar, in Proceedings of the 17th IEEE International Pulsed Power Conference, Washington, DC, 2009 (Ref. [10]), p. 425.

[16] K. R. LeChien, W. A. Stygar, M. E. Savage, P. E. Wakeland, V. Anaya, D. S. Artery, M. J. Baremore, D. E. Bliss, R. Chavez, G. D. Coombs, J. P. Corley, P. A. Jones, A. K. Kipp, B. A. Lewis, J. A. Lott, J. J. Lynch, G. R. McKee, S. D. Ploor, K. R. Prestwich, S. A. Roznowski, S. D. White, and J. R. Woodworth (unpublished).

[17] R. B. Spielman, W. A. Stygar, J. F. Seamen, F. Long, H. Ives, R. Garcia, T. Wagoner, K. W. Struve, M. Mostrom, I. Smith, P. Spence, and P. Corcoran, in Proceedings of the 11th IEEE International Pulsed Power Conference, Baltimore, MD, 1997 (Ref. [1]), p. 709.

[18] P. A. Corcoran, J. W. Douglas, I. D. Smith, P. W. Spence, W. A. Stygar, K. W. Struve, T. H. Martin, R. B. Spielman, and H. C. Ives, in Proceedings of the 11th IEEE International Pulsed Power Conference, Baltimore, MD, 1997 (Ref. [1]), p. 466.

[19] H. C. Ives, D. M. Van De Valde, F. W. Long, J. W. Smith, R. B. Spielman, W. A. Stygar, R. W. Wavrik, and R. W. Shoup, in Proceedings of the 11th IEEE International Pulsed Power Conference, Baltimore, MD, 1997 (Ref. [1]), p. 1602.

[20] W. A. Stygar, R. B. Spielman, G. O. Allshouse, C. Deeney, D. R. Humphries, H. C. Ives, F. W. Long, T. H. Martin, M. K. Matzen, D. H. McDaniel, C. W. Mendel, Jr., L. P. Mix, T. J. Nash, J. W. Poukey, J. J. Ramirez, T. W. L. Sanford, J. F. Seamen, D. B. Seidel, J. W. Smith, D. M. Van De Valde, R. W. Wavrik, P. A. Corcoran, J. W. Douglas, I. D. Smith, M. A. Mostrom, K. W. Struve, T. P. Hughes, R. E. Clark, R. W. Shoup, T. C. Wagoner, T. L. Gilliland, and B. P. Peyton, in Proceedings of the 11th IEEE International Pulsed Power Conference, Baltimore, MD, 1997 (Ref. [1]), p. 591.

[21] R. B. Spielman, C. Deeney, G. A. Chandler, M. R. Douglas, D. L. Fehl, M. K. Matzen, D. H. McDaniel, T. J. Nash, J. L. Porter, T. W. L. Sanford, J. F. Seaman, W. A.

Stygar, K. W. Struve, S. P. Breeze, J. S. McGurn, J. A. Torres, D. M. Zagar, T. L. Gilliland, D. O. Jobe, J. L. McKenney, R. C. Mock, M. Vargas, and T. Wagoner, Phys. Plasmas **5**, 2105 (1998).

[22] W. A. Stygar, P. A. Corcoran, H. C. Ives, R. B. Spielman, J. W. Douglas, B. A. Whitney, M. A. Mostrom, T. C. Wagoner, C. S. Speas, T. L. Gilliland, G. A. Allshouse, R. E. Clark, G. L. Donovan, T. P. Hughes, D. R. Humphreys, D. M. Jaramillo, M. F. Johnson, J. W. Kellogg, R. J. Leeper, F. W. Long, T. H. Martin, T. D. Mulville, M. D. Pelock, B. P. Peyton, J. W. Poukey, J. J. Ramirez, P. G. Reynolds, J. F. Seamen, D. B. Seidel, A. P. Seth, A. W. Sharpe, R. W. Shoup, J. W. Smith, D. M. Van De Valde, and R. W. Wavrik, Phys. Rev. ST Accel. Beams **12**, 120401 (2009).

[23] D. D. Ryutov, M. S. Derzon, and M. K. Matzen, Rev. Mod. Phys. **72**, 167 (2000).

[24] M. K. Matzen, Phys. Plasmas **4**, 1519 (1997).

[25] M. A. Liberman, J. S. DeGroot, A. Toor, and R. B. Spielman, *Physics of High-Density Z-Pinch Plasmas* (Springer, New York, 1999).

[26] D. B. Reisman, A. Toor, R. C. Cauble, C. A. Hall, J. R. Asay, M. D. Knudson, and M. D. Furnish, J. Appl. Phys. **89**, 1625 (2001).

[27] J. R. Asay and M. D. Knudson, in *High-Pressure Shock Compression of Solids VIII: The Science and Technology of High-Velocity Impact*, edited by L. C. Chhabildas, L. Davison, and Y. Horie (Springer, New York, 2005), p. 329.

[28] M. D. Knudson, C. A. Hall, R. Lemke, C. Deeney, and J. R. Asay, Int. J. Impact Engng. **29**, 377 (2003).

[29] R. W. Lemke, M. D. Knudson, D. E. Bliss, K. Cochrane, J.-P. Davis, A. A. Giunta, H. C. Harjes, and S. A. Slutz, J. Appl. Phys. **98**, 073530 (2005).

[30] C. L. Ruiz, G. W. Cooper, S. A. Slutz, J. E. Bailey, G. A. Chandler, T. J. Nash, T. A. Mehlhorn, R. J. Leeper, D. Fehl, A. J. Nelson, J. Franklin, and L. Ziegler, Phys. Rev. Lett. **93**, 015001 (2004).

[31] W. A. Stygar, H. C. Ives, D. L. Fehl, M. E. Cuneo, M. G. Mazarakis, J. E. Bailey, G. R. Bennett, D. E. Bliss, G. A. Chandler, R. J. Leeper, M. K. Matzen, D. H. McDaniel, J. S. McGurn, J. L. McKenney, L. P. Mix, D. J. Muron, J. L. Porter, J. J. Ramirez, L. E. Ruggles, J. F. Seamen, W. W. Simpson, C. S. Speas, R. B. Spielman, K. W. Stuve, J. A. Torres, R. A. Vesey, T. C. Wagoner, T. L. Gilliland, M. L. Horry, D. O. Jobe, S. E. Lazier, J. A. Mills, T. D. Mulville, J. H. Pyle, T. M. Romero, J. J. Seamen, and R. M. Smelser, Phys. Rev. E **69**, 046403 (2004).

[32] W. A. Stygar, M. E. Cuneo, R. A. Vesey, H. C. Ives, M. G. Mazarakis, G. A. Chandler, D. L. Fehl, R. J. Leeper, M. K. Matzen, D. H. McDaniel, J. S. McGurn, J. L. McKenney, D. J. Muron, C. L. Olson, J. L. Porter, J. J. Ramirez, J. F. Seamen, C. S. Speas, R. B. Spielman, K. W. Struve, J. A. Torres, E. M. Waisman, T. C. Wagoner, and T. L. Gilliland, Phys. Rev. E **72**, 026404 (2005).

[33] M. E. Cuneo, E. M. Waisman, S. V. Lebedev, J. P. Chittenden, W. A. Stygar, G. A. Chandler, R. A. Vesey, E. P. Yu, T. J. Nash, D. E. Bliss, G. S. Sarkisov, T. C. Wagoner, G. R. Bennett, D. B. Sinars, J. L. Porter, W. W. Simpson, L. E. Ruggles, D. F. Wenger, C. J. Garasi, B. V. Oliver, R. A. Aragon, W. E. Fowler, M. C. Hettrick, G. C. Idzorek, D. Johnson, K. Keller, S. E. Lazier, J. S. McGurn,

T. A. Mehlhorn, T. Moore, D. S. Nielsen, J. Pyle, S. Speas, K. W. Struve, and J. A. Torres, Phys. Rev. E **71**, 046406 (2005).

[34] M. E. Cuneo, R. A. Vesey, J. H. Hammer, J. L. Porter, Jr., L. E. Ruggles, and W. W. Simpson, Laser Part. Beams **19**, 481 (2001).

[35] M. E. Cuneo, R. A. Vesey, G. R. Bennett, D. B. Sinars, W. A. Stygar, E. M. Waisman, J. L. Porter, P. K. Rambo, I. C. Smith, S. V. Lebedev, J. P. Chittenden, D. E. Bliss, T. J. Nash, G. A. Chandler, B. B. Afeyan, E. P. Yu, R. B. Campbell, R. G. Adams, D. L. Hanson, T. A. Mehlhorn, and M. K. Matzen, Plasma Phys. Controlled Fusion **48**, R1 (2006).

[36] C. L. Olson, *Landholt-Boerstein Handbook on Energy Technologies* (Springer, Berlin, 2004), Vol. 8, p. 3.

[37] S. A. Slutz, M. C. Herrmann, R. A. Vesey, A. B. Sefkow, D. B. Sinars, D. C. Rovang, K. J. Peterson, and M. E. Cuneo (unpublished).

[38] D. Sinars, S. Slutz, H. Herrmann, K. Peterson, R. Vesey, and B. Blue, Bull. Am. Phys. Soc. **54**, 100 (2009).

[39] B. Jones, C. Coverdale, C. Deeney, D. Sinars, E. Waisman, M. Cuneo, D. Ampleford, P. LePell, K. Cochrane, J. Thornhill, J. Apruzese, A. Dasgupta, K. Whitney, R. Clark, and J. Chittenden, Phys. Plasmas **15**, 122703 (2008).

[40] J. E. Bailey, G. A. Chandler, D. Cohen, M. E. Cuneo, M. E. Foord, R. F. Heeter, D. Jobe, P. W. Lake, J. J. MacFarlane, T. J. Nash, D. S. Nielson, R. Smelser, and J. Torres, Phys. Plasmas **9**, 2186 (2002).

[41] G. A. Rochau, J. E. Bailey, Y. Maron, G. A. Chandler, G. S. Dunham, D. V. Fisher, V. I. Fisher, R. W. Lemke, J. J. MacFarlane, K. J. Peterson, D. G. Schroen, S. A. Slutz, and E. Stambulchik, Phys. Rev. Lett. **100**, 125004 (2008).

[42] J. E. Bailey, G. A. Rochau, R. C. Mancini, C. A. Iglesias, J. J. MacFarlane, I. E. Golovkin, C. Blancard, Ph. Cosse, and G. Faussurier, Phys. Plasmas **16**, 058101 (2009).

[43] M. D. Knudson, D. L. Hanson, J. E. Bailey, C. A. Hall, J. R. Asay, and C. Deeney, Phys. Rev. B **69**, 144209 (2004).

[44] J.-P. Davis, C. Deeney, M. D. Knudson, R. W. Lemke, T. D. Pointon, and D. E. Bliss, Phys. Plasmas **12**, 056310 (2005).

[45] D. H. Dolan, M. D. Knudson, C. A. Hall, and C. Deeney, Nature Phys. **3**, 339 (2007).

[46] J. E. Bailey, M. D. Knudson, A. L. Carlson, G. S. Dunham, M. P. Desjarlais, D. L. Hanson, and J. R. Asay, Phys. Rev. B **78**, 144107 (2008).

[47] W. A. Stygar, S. E. Rosenthal, H. C. Ives, T. C. Wagoner, G. O. Allshouse, K. E. Androlewicz, G. L. Donovan, D. L. Fehl, M. H. Frese, T. L. Gilliland, M. F. Johnson, J. A. Mills, D. B. Reisman, P. G. Reynolds, C. S. Speas, R. B. Spielman, K. W. Struve, A. Toor, and E. M. Waisman, Phys. Rev. ST Accel. Beams **11**, 120401 (2008).

[48] M. K. Matzen, M. A. Sweeney, R. G. Adams, J. R. Asay, J. E. Bailey, G. R. Bennett, D. E. Bliss, D. D. Bloomquist, T. A. Brunner, R. B. Campbell, G. A. Chandler, C. A. Coverdale, M. E. Cuneo, J.-P. Davis, C. Deeney, M. P. Desjarlais, G. L. Donovan, C. J. Garasi, T. A. Haill, C. A. Hall, D. L. Hanson, M. J. Hurst, B. Jones, M. D. Knudson, R. J. Leeper, R. W. Lemke, M. G. Mazarakis, D. H. McDaniel, T. A. Mehlhorn, T. J. Nash, C. L. Olson, J. L. Porter, P. K. Rambo, S. E. Rosenthal, G. A. Rochau, L. E.

Ruggles, C. L. Ruiz, T. W. L. Sanford, J. F. Seamen, D. B. Sinars, S. A. Slutz, I. C. Smith, K. W. Struve, W. A. Stygar, R. A. Vesey, E. A. Weinbrecht, D. F. Wenger, and E. P. Yu, Phys. Plasmas **12**, 055503 (2005).

[49] LSP is a software product developed by ATK Mission Research, Albuquerque, NM 87110, with initial support from the Department of Energy SBIR Program.

[50] C. K. Birdsall and A. B. Langdon, *Plasma Via Computer Simulation* (Adam Hilger, New York, 1991).

[51] R. W. Hockney and J. W. Eastwood, *Computer Simulation Using Particles* (Adam Hilger, New York, 1988).

[52] D. D. Hinshelwood, Naval Research Laboratory Memorandum Report No. 5185, 1983.

[53] W. A. Stygar, W. E. Fowler, K. R. LeChien, F. W. Long, M. G. Mazarakis, G. R. KcKee, J. L. KcKenney, J. L. Porter, M. E. Savage, B. S. Stoltzfus, D. M. Van De Valde, and J. R. Woodworth, Phys. Rev. ST Accel. Beams **12**, 030402 (2009).

[54] W. A. Stygar, M. E. Cuneo, D. I. Headley, H. C. Ives, R. J. Leeper, M. G. Mazarakis, C. L. Olson, J. L. Porter, and T. C. Wagoner, Phys. Rev. ST Accel. Beams **10**, 030401 (2007).

[55] D. V. Rose, D. R. Welch, B. V. Oliver, J. J. Leckbee, J. E. Maenchen, D. L. Johnson, A. A. Kim, B. M. Kovalchuk, and V. A. Sinebryukhov, IEEE Trans. Plasma Sci. **34**, 1879 (2006).

[56] B. V. Oliver, T. C. Genoni, D. L. Johnson, V. L. Bailey, P. Corcoran, I. Smith, J. E. Maenchen, I. Molina, and K. Hahn, in *Proceedings of the 14th IEEE International Pulsed Power Conference, Dallas, TX, 2003*, edited by M. Giesselmann and A. Neuber (IEEE, Piscataway, NJ, 2003), p. 395.

[57] N. Bruner, T. Genoni, E. Madrid, D. Rose, D. Welch, K. Hahn, J. Leckbee, S. Portillo, B. Oliver, V. Bailey, and D. Johnson, Phys. Rev. ST Accel. Beams **11**, 040401 (2008).

[58] N. Bruner, T. Genoni, E. Madrid, D. Welch, K. Hahn, and B. Oliver, Phys. Rev. ST Accel. Beams **12**, 070401 (2009).

[59] P. F. Ottinger and J. W. Schumer, Phys. Plasmas **13**, 063101 (2006).

[60] P. F. Ottinger and J. W. Schumer, Phys. Plasmas **13**, 063109 (2006).

[61] J. W. Schumer, P. F. Ottinger, and C. L. Olson, IEEE Trans. Plasma Sci. **34**, 2652 (2006).

[62] P. F. Ottinger and J. W. Schumer, IEEE Trans. Plasma Sci. **35**, 154 (2007).

[63] V. Bailey, P. Corcoran, V. Carboni, I. Smith, D. L. Johnson, B. Oliver, K. Thomas, and M. Swiekosz, in *Proceedings of the 15th IEEE International Pulsed Power Conference, Monterey, CA, 2005*, edited by J. Maenchen and E. Schamiloglu (IEEE, Piscataway, NJ, 2005), p. 322.

[64] V. L. Bailey, P. Corcoran, D. L. Johnson, I. Smith, B. Oliver, and J. Maenchen, in Proceedings of the 16th IEEE Pulsed Power and Plasma Science Conference, Albuquerque, NM, 2007 (Ref. [7]), p. 1268.

[65] http://www.dell.com.

[66] http://www.intel.com.

[67] http://www.infinibandta.org.

[68] W. A. Stygar, M. E. Savage, T. C. Wagoner, L. F. Bennett, J. P. Corley, G. L. Donovan, D. H. Fehl, H. C. Ives, K. R. LeChien, G. T. Leifeste, F. W. Long, R. G. McKee, J. A. Mills, J. K. Moore, J. J. Ramirez, B. S. Stoltzfus, K. W.

Struve, and J. R. Woodworth, Phys. Rev. ST Accel. Beams **12**, 010402 (2009).

[69] M. A. Kemp, R. D. Curry, J. M. Gahl, K. F. McDonald, and K. W. Struve, IEEE Trans. Plasma Sci. **33**, 1245 (2005).

[70] M. A. Kemp, R. D. Curry, and S. D. Kovaleski, IEEE Trans. Plasma Sci. **34**, 95 (2006).

[71] D. L. Johnson, J. P. VanDevender, and T. H. Martin, IEEE Trans. Plasma Sci. **8**, 204 (1980).

[72] J. R. Woodworth, J. M. Lehr, J. Elizondo-Decanini, P. A. Miller, P. Wakeland, M. Kincy, J. Garde, B. Aragon, W. Fowler, G. Mowrer, J. E. Maenchen, G. S. Sarkisov, J. Corley, K. Hodge, S. Drennan, D. Guthrie, M. Navarro, D. L. Johnson, H. C. Ives, M. J. Slattery, and D. A. Muirhead, IEEE Trans. Plasma Sci. **32**, 1778 (2004).

[73] M. K. Matzen, in Proceedings of the 16th IEEE Pulsed Power and Plasma Science Conference, Albuquerque, NM, 2007 (Ref. [7]), p. 1.

[74] M. K. Matzen, B. W. Atherton, M. E. Cuneo, G. L. Donovan, C. A. Hall, M. Hermann, M. L. Kiefer, R. J. Leeper, G. T. Leifeste, F. W. Long, G. R. McKee, T. A. Mehlhorn, J. L. Porter, L. X. Schneider, K. W. Struve, W. A. Stygar, and E. A. Weinbrecht, Acta Phys. Pol. A **115**, 956 (2009).

[75] K. W. Struve, L. F. Bennett, J. P. Davis, D. D. Hinshelwood, M. E. Savage, B. S. Stoltzfus, and T. C. Wagoner, in Proceedings of the 17th IEEE International Pulsed Power Conference, Washington, DC, 2009 (Ref. [10]), p. 1147.

[76] T. W. L. Sanford, R. W. Lemke, R. C. Mock, G. A. Chandler, R. J. Leeper, C. L. Ruiz, D. L. Peterson, R. E. Chrien, G. C. Idzorek, R. G. Watt, and J. P. Chittenden, Phys. Plasmas **9**, 3573 (2002).

[77] J. E. Bailey, G. A. Chandler, R. C. Mancini, S. A. Slutz, G. A. Rochau, M. Bump, T. J. Buris-Mog, G. Cooper, G. Dunhan, I. Golovkin, J. D. Kilkenny, P. W. Lake, R. J. Leeper, R. Lemke, J. J. MacFarlane, T. A. Mehlhorn, T. C. Moore, T. J. Nash, A. Nikroo, D. S. Nielsen, K. L. Peterson, C. L. Ruiz, D. G. Schroen, D. Steinman, and W. Varnum, Phys. Plasmas **13**, 056301 (2006).

[78] S. A. Slutz, K. J. Peterson, R. A. Vesey, R. W. Lemke, J. E. Bailey, W. Varnum, C. L. Ruiz, G. W. Cooper, G. A. Chandler, G. A. Rochau, and T. A. Mehlhorn, Phys. Plasmas **13**, 102701 (2006).

[79] G. A. Rochau, J. E. Bailey, G. A. Chandler, G. Cooper, G. S. Dunham, P. W. Lake, R. J. Leeper, R. W. Lemke, T. A. Mehlhorn, A. Nikroo, K. J. Peterson, C. L. Ruiz, D. G. Schroen, S. A. Slutz, D. Steinman, W. A. Stygar, and W. Varnum, Plasma Phys. Controlled Fusion **49**, B591 (2007).

[80] W. N. Weseloh, in *Proceedings of the 7th IEEE Pulsed Power Conference, Monterey, CA, 1989*, edited by R. White and B. H. Bernstein (IEEE, Piscataway, NJ, 1989), p. 43.

[81] T. C. Wagoner, W. A. Stygar, H. C. Ives, T. L. Gilliland, R. B. Spielman, M. F. Johnson, P. G. Reynolds, J. K. Moore, R. L. Morning, D. L. Fehl, K. E. Androlewicz, J. E. Bailey, R. S. Broyles, T. A. Dinwoodie, G. L. Donovan, M. E. Dudley, K. D. Hahn, A. A. Kim, J. R. Lee, R. J. Leeper, G. T. Leifeste, J. A. Melville, J. A. Mills, L. P. Mix, W. B. S. Moore, B. P. Peyton, J. L. Porter, G. A. Rochau, G. E. Rochau, M. E. Savage, J. F. Seamen, J. D. Serrano, A. W. Sharpe, R. W. Shoup, J. S. Slopek, C. S. Speas, K. W. Struve, D. M. Van De Valde, and R. M. Woodring, Phys. Rev. ST Accel. Beams **11**, 100401 (2008).

[82] S. E. Rosenthal, M. P. Desjarlais, R. B. Spielman, W. A. Stygar, J. R. Asay, M. R. Douglas, C. A. Hall, M. H. Frese, R. L. Morse, and D. B. Reisman, IEEE Trans. Plasma Sci. **28**, 1427 (2000).